Taylor & Francis
Taylor & Francis Group

Machining Science and Technology
An International Journal

ISSN: 1091-0344 (Print) 1532-2483 (Online) Journal homepage: http://www.tandfonline.com/loi/lmst20

AN ANALYTICAL MODEL OF OBLIQUE CUTTING WITH APPLICATION TO END MILLING

Binglin Li , Yujin Hu , Xuelin Wang , Chenggang Li & Xingxing Li

To cite this article: Binglin Li , Yujin Hu , Xuelin Wang , Chenggang Li & Xingxing Li (2011) AN ANALYTICAL MODEL OF OBLIQUE CUTTING WITH APPLICATION TO END MILLING, Machining Science and Technology, 15:4, 453-484, DOI: 10.1080/10910344.2011.620920

To link to this article: http://dx.doi.org/10.1080/10910344.2011.620920

Machining Science and Technology, 15:453–484

ISSN: 1091-0344 print/1532-2483 online
DOI: 10.1080/10910344.2011.620920

Taylor & Francis
Taylor & Francis Group

AN ANALYTICAL MODEL OF OBLIQUE CUTTING WITH APPLICATION TO END MILLING

Binglin Li, Yujin Hu, Xuelin Wang, Chenggang Li, and Xingxing Li
School of Mechanical Science and Engineering, Huazhong University of Science and Technology, Wuhan, China

□ *A new analytical cutting force model is presented for oblique cutting. Orthogonal cutting theory based on unequal division shear zone is extended to oblique cutting using equivalent plane approach. The equivalent plane angle is defined to determine the orientation of the equivalent plane. The governing equations of chip flow through the primary shear zone are established by introducing a piecewise power law distribution assumption of shear strain rate. The flow stress is calculated from Johnson-cook material constitutive equation. The predictions were compared with test data from the available literature and showed good correlation. The proposed model of oblique cutting was applied to predict the cutting forces in end milling. The helical flutes are decomposed into a set of differential oblique cutting edges. To every engaged tooth element, the differential cutting forces are obtained from oblique cutting process. Experiments on machining AISI 1045 steel under different cutting conditions were conducted to validate the proposed model. It shows that the predicted cutting forces agree with the measurements both in trends and values.*

Keywords analytical model, cutting force, end milling, flow stress, oblique cutting

INTRODUCTION

The prediction of cutting forces is essential to improve reliability, accuracy and productivity in metal cutting. In fact, it can be used as fundamental data for cutter deflection, tool wear and breakage, surface integrity, selecting appropriate process parameters and designing better fixtures, etc.

At present, prediction model of cutting force is usually restricted to the relatively simple case of orthogonal cutting in which the cutting edge is set normal to the cutting velocity. Nevertheless, machining processes encountered in practice are often oblique. To study these machining operations

Address correspondence to Yujin Hu, Department of Mechanical Design, School of Mechanical Science and Engineering, Huazhong University of Science and Technology, Wuhan, Hubei Province 430074, China. E-mail: yjhu2787@yahoo.com.cn

with complex cutting edge such as milling, the helical edge can be considered as a set of infinitesimal oblique cutting elements. So the study of oblique cutting process is regarded as a critical step.

Some models of oblique cutting have been developed using mechanistic, analytical, numerical methods. In the mechanistic method, cutting force is supposed to be proportional to the chip load. The constants of proportionality are called specific cutting coefficients and must be determined from experimental data. Most of the past research in milling is focusing on cutting force prediction using the mechanistic approach (Sabberwal, 1960; Smith and Tlusty, 1991; Yang and Park, 1991; Budak et al., 1996; Yun and Cho, 2001; Lazoglu, 2003). In this type of models, the cutting force is estimated by dividing the cutting edge into small elements and applying a simple mathematical formulation of oblique cutting to each of these. Cutting force is calculated based on the undeformed chip thickness, cutting conditions and several specific cutting coefficients. An important aspect for the accuracy of force prediction is calibration and fitting of the specific cutting coefficients from a set of experimental tests previously carried out, orthogonal or oblique turning tests or directly milling tests with varying cutter geometry, cutting conditions, workpiece material properties. This approach has demonstrated that orthogonal or oblique cutting force data may be successfully used in the calculation of cutting forces. But a large amount of data must be gathered and stored in the cutting databases. Another shortcoming of the databases is that they do not provide physical mechanism on the cutting processes.

Typical approach for numerical modeling is finite element method (FEM). At the early stage of finite element (FE) models most are limited to the two-dimensional case of orthogonal cutting. Recent advances in software technology have made it possible to run three-dimensional simulation (example for the commercial code–AdvantEdge). Lin and Lin (1999), Llanos et al. (2009) and others tried to develop and improve the oblique cutting models by the three-dimensional FEM. In recent years, the effort is dedicated to develop the arbitrary Lagrangian-Eulerian (ALE) formulation (Llanos et al., 2009) to FE model. Currently available FE models can be used to predict cutting forces, stress and temperature distributions, tool wear rates, chip morphology and breakage, and residual stress. Simulations of FEM are very time consuming and the accuracy of results always need be improved.

Many efforts have long been devoted to develop analytical models. Merchant (1944) first developed the single-shear plane model of oblique cutting. This model analysed the geometric relation between the shear and the chip flow directions. Shaw et al. (1952) emphasized the physical significance of working in the equivalent plane for oblique cutting. Using the equivalent plane approach, Morcos (1980) generalized Lee and

Shaffer's slip line field solution to oblique cutting. Usui et al. (1978) proposed an energy approach with a relatively approximate good result. The total work was calculated as the sum of shear work and friction work, the chip flow angle and normal shear plane angle were found by minimizing the total energy with respect to the chip flow angle. Stephenson and Wu (1988) proposed an upper bound model for oblique cutting based on numerical minimization of a weighted sum of plastic work and frictional work.

Armarego and Whitfield (1985), using the single-shear plane model and assuming the chip length ratio in the oblique cutting is the same as that in orthogonal cutting from their experiments, obtained the normal shear angle from the chip length ratio. Shamato and Altintas (1999) proposed a theoretical shear angle prediction approach in oblique machining by employing either the maximum shear stress or the minimum energy principle. The basic assumption that the deformation occurs on a single-shear plane produces a velocity discontinuity along which the strain rate is infinite. Although geometric arguments can be used to compute an average effective strain rate, this assumption makes it difficult include strain rate hardening, which is known to be a significant factor in high speed deformation processes.

Oxley (1989) introduced a new parallel-sided shear zone model for the machining predictive theory. Oxley not only used the geometric method, but also considered the influence of temperature, strain rate and strain on flow stress. Flow stress calculation is essential to the prediction of cutting force. It can be obtained mainly by using three methods: first, the flow stress is computed from the measured cutting force. The cutting force coefficient and edge force coefficient proposed by Altintas and his co-workers (2000a, 2000b) is the extension of this approach.

Second, the flow stress is obtained from finite element calculations that used mathematical theories and non-linear numerical algorithms to model plastic flow, heat conduction, thermomechanical coupling. Third, the flow stress is predicted using analytical method by establishing the governing equations of chip formation. In other words, the first one directly computes flow stress by using inverse method, which needs some additional cutting tests. The last two indirectly derive flow stress from analytical model or finite element model from material constitutive relationship using forward method.

The material constitutive equation can be experimentally identified from high-speed compression tests, cutting tests, and Split–Hopkinson's Pressure Bar (SHPB) tests. Lin et al. (1982) extended Oxley's orthogonal cutting model to oblique machining. Despite the obvious improvements in Oxley and Lin's model, it requires the inputs flow stress data of the work material.

Unfortunately, such relations are only available in the literature for low carbon steel. Adibi-Sedeh et al. (2003) extended Oxley's machining theory with Johnson-Cook material model. Moufki et al. (2000) developed

a thermomechanical model of oblique cutting for high speed machining. This model makes an assumption that hydrostatic pressure is constant in the primary shear zone, so that the motion equation reduces to a single relation by calculating the inertial term. Budak and Ozlu (2008) modified Moufki's model in which the rake contact is represented by two regions of respectively sticking and sliding friction. Fontaine et al. (2006) applied Moufki's model to cutting force prediction in ball-end milling. However, plastic deformation of metal cutting process at general cutting speed is regarded as quasi-static, since it is assumed that inertial forces due to the plastic flow may be neglected (Johnson and Mellor, 1983).

In this study, a new analytical model for oblique cutting is presented based on the unequal division shear zone model. The orthogonal cutting theory proposed by Li et al. (2011) is extended to oblique cutting using equivalent plane approach. The governing equations of chip flow through the primary shear zone are established by introducing a piecewise power law distribution assumption of the shear strain rate. The cutting forces are calculated from Johnson-Cook material constitutive equation. The proposed model is applied to cutting force prediction in end milling. In the same way as that in a mechanistic approach, the end milling operation is carried out by a series of small oblique cutting process.

This paper is organized as follows. The geometrical and kinematical characterizations of oblique cutting are discussed first. The governing equations of chip flow through the primary shear zone are established next. The calculated expressions of cutting forces for the use of the model are detailed in the next section. Then, the predictive model for end milling using the proposed oblique cutting approach is introduced. Predicted results are compared with the oblique cutting test data from the available literature, and an end milling experiment is performed to verify that the proposed approach is applicable to the machining operations modeling with the complex cutting edge.

GEOMETRICAL CHARACTERIZATION OF OBLIQUE CUTTING

Figure 1 illustrates the process of oblique cutting. The cutting thickness t, cutting width b, cutting speed V, normal rake angle γ_n, and inclination angle λ_s are known. To study the geometries, kinematics, and forces relationships of oblique cutting, a set of coordinate systems are defined. These coordinate systems are associated to the reference planes, and are summarized as follows (see Fig. 2):

- Frame $(\mathbf{x_o}, \mathbf{y_o}, \mathbf{z_o})$ $\mathbf{x_o}$ is parallel to the cutting velocity direction, $(\mathbf{y_o}, \mathbf{z_o})$ is the reference plane P_r, $(\mathbf{x_o}, \mathbf{y_o})$ is the cutting plane P_s.

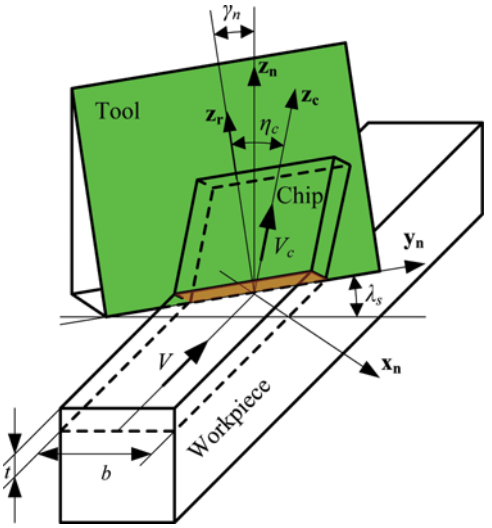

FIGURE 1 The schematic diagram of oblique cutting. (Figure available in color online.)

- Frame ($\mathbf{x_n}$, $\mathbf{y_n}$, $\mathbf{z_n}$) $\mathbf{y_n}$ is the cutting edge direction, ($\mathbf{x_n}$, $\mathbf{z_n}$) is the cutting plane P_s, $\mathbf{z_n}$ is parallel to $\mathbf{z_o}$.
- Frame ($\mathbf{x_r}$, $\mathbf{y_r}$, $\mathbf{z_r}$) $\mathbf{y_r}$ is collinear to $\mathbf{y_n}$, ($\mathbf{y_r}$, $\mathbf{z_r}$) is the rake face A_γ, $\mathbf{z_r}$ is perpendicular to $\mathbf{y_r}$.
- Frame (**x, y, z**) **y** is collinear to $\mathbf{y_n}$, (**x, z**) is the normal plane P_n, **z** is perpendicular to the shear plane P_{sh}.

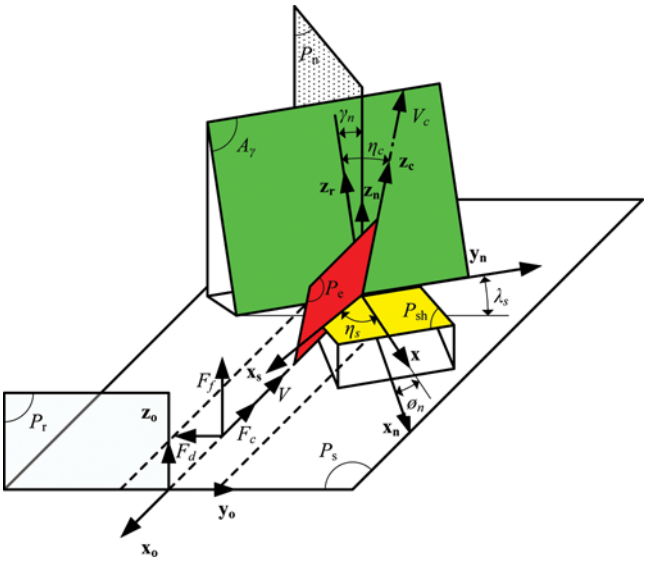

FIGURE 2 The geometrical relationship of oblique cutting. (Figure available in color online.)

- Frame $(\mathbf{x_c}, \mathbf{y_c}, \mathbf{z_c})$ $\mathbf{z_c}$ is the chip flow direction, $(\mathbf{y_c}, \mathbf{z_c})$ is the rake face A_γ, $\mathbf{x_c}$ is collinear to $\mathbf{x_r}$.
- Frame $(\mathbf{x_s}, \mathbf{y_s}, \mathbf{z_s})$ $\mathrm{x_s}$ is the shear flow direction, $(\mathbf{x_s}, \mathbf{y_s})$ is the shear plane P_{sh}, $\mathbf{z_s}$ is collinear to $\mathbf{z}$.
- Frame $(\mathbf{x_e}, \mathbf{y_e}, \mathbf{z_e})$ $\mathbf{x_e}$ is collinear to $\mathbf{x_s}$, $(\mathbf{x_e}, \mathbf{z_e})$ is the equivalent plane P_{e}, $\mathbf{y_e}$ is perpendicular to the equivalent plane P_{e}.

The preceding seven frames can be related by rotation transformation, as shown in Figure 3. For instance, $(\mathbf{x_n}, \mathbf{y_n}, \mathbf{z_n})$ is obtained by the rotation of angle λ_s of the frame $(\mathbf{x_o}, \mathbf{y_o}, \mathbf{z_o})$ around the $\mathbf{z_o}$ axis, which is expressed as the following form: $(\mathbf{x_o}, \mathbf{y_o}, \mathbf{z_o}) \xrightarrow{\mathrm{R}(\mathbf{z_o}, \lambda_s)} (\mathbf{x_n}, \mathbf{y_n}, \mathbf{z_n})$. The rest can be given by analogy. $\varnothing_n$ is the normal shear angle, η_c is the chip flow angle, η_s is the shear flow angle, η_e is equivalent plane angle. Because the shear plane P_{sh} isn't perpendicular to the equivalent plane P_{e}, the equivalent plane angle η_e is defined to connect P_{sh} to P_{e}.

According to the coordinate transformation, the components of the units associated with this research are given by

$$\mathbf{x} = \cos\lambda_s \cos\phi_n \mathbf{x_o} + \sin\lambda_s \cos\phi_n \mathbf{y_o} + \sin\phi_n \mathbf{z_o} \tag{1}$$

$$\mathbf{y} = -\sin\lambda_s \mathbf{x_o} + \cos\lambda_s \mathbf{y_o} \tag{2}$$

$$\mathbf{z} = -\cos\lambda_s \sin\phi_n \mathbf{x_o} - \sin\lambda_s \sin\phi_n \mathbf{y_o} + \cos\phi_n \mathbf{z_o} \tag{3}$$

$$\mathbf{x_c} = \cos(\phi_n - \gamma_n)\mathbf{x} - \sin(\phi_n - \gamma_n)\mathbf{z} \tag{4}$$

$$\begin{aligned}\mathbf{z_c} &= \sin(\phi_n - \gamma_n)\cos\eta_c \mathbf{x} + \sin\eta_c \mathbf{y} + \cos(\phi_n - \gamma_n)\cos\eta_c \mathbf{z} \\ &= (\sin(\phi_n - \gamma_n)\cos\eta_c \cos\eta_s - \sin\eta_c \sin\eta_s)\mathbf{x}_s \\ &\quad + (\sin(\phi_n - \gamma_n)\cos\eta_c \sin\eta_s + \sin\eta_c \cos\eta_s)\mathbf{y}_s + \sin(\phi_n - \gamma_n)\cos\eta_c \mathbf{z}_s\end{aligned} \tag{5}$$

$$\mathbf{x_s} = \cos\eta_s \mathbf{x} - \sin\eta_s \mathbf{y} \tag{6}$$

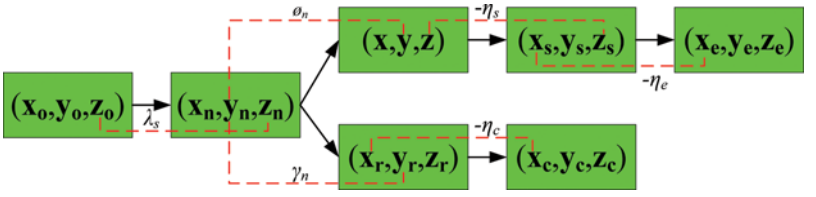

FIGURE 3 The rotational transformation relationships between the coordinate systems. (Figure available in color online.)

KINEMATICAL CHARACTERIZATION OF OBLIQUE CUTTING

Generally, two approaches have been used to model oblique cutting process. One of them is the normal plane method (Armarego and Whitfield, 1985; Oxley, 1989; Altintas, 2000a; Moufki et al., 2000). Many researchers made the assumption that mechanistic analysis of oblique cutting in the normal plane is equivalent to that of orthogonal cutting, and then all the velocity and force vectors are projected on the normal plane. The other is the equivalent plane method (Shaw et al., 1952; Usui et al., 1978; Morcos, 1980; Rao and Shin, 2002). The equivalent plane is determined by the cutting velocity and chip velocity, the mechanism of oblique cutting is considered as the accumulation of a series of two dimensional cutting processes. The latter method is adopted in this paper. In order to locate the equivalent plane, the equivalent plane angle is defined by the following expressions

$$\tan \eta_e = \frac{\mathbf{z_e} \times \mathbf{z_s}}{\mathbf{z_e} \times \mathbf{y_s}} = \frac{\tan \eta_c \cos \eta_s + \sin(\phi_n - \gamma_n) \sin \eta_s}{\cos(\phi_n - \gamma_n)} \tag{7}$$

The cutting and chip direction can be expressed as

$$\begin{aligned}\mathbf{x_o} = {} & (\cos \phi_n \cos \lambda_s \cos \eta_s + \sin \lambda_s \sin \eta_s)\mathbf{x_e} \\ & + (\cos \lambda_s \cos \phi_n \sin \eta_s \cos \eta_e - \sin \lambda_s \cos \eta_s \cos \eta_e + \cos \lambda_s \sin \phi_n \sin \eta_e)\mathbf{y_e} \\ & + (\cos \lambda_s \cos \phi_n \sin \eta_s \sin \eta_e - \sin \lambda_s \cos \eta_s \sin \eta_e - \cos \lambda_s \sin \phi_n \cos \eta_e)\mathbf{z_e}\end{aligned} \tag{8}$$

$$\begin{aligned}\mathbf{z_c} = {} & (\sin(\phi_n - \gamma_n) \cos \eta_c \cos \eta_s - \sin \eta_c \sin \eta_s)\mathbf{x_e} \\ & + (\sin(\phi_n - \gamma_n) \cos \eta_c \sin \eta_s \cos \eta_e + \sin \eta_c \cos \eta_s \cos \eta_e \\ & \quad - \cos(\phi_n - \gamma_n) \cos \eta_c \sin \eta_e)\mathbf{y_e} \\ & + (\sin(\phi_n - \gamma_n) \cos \eta_c \sin \eta_s \sin \eta_e + \sin \eta_c \cos \eta_s \sin \eta_e \\ & + \cos(\phi_n - \gamma_n) \cos \eta_c \cos \eta_e)\mathbf{z_e}\end{aligned} \tag{9}$$

According to the equivalent plane through $\mathbf{x}_o$, the projection component of $\mathbf{x}_o$ in the direction $\mathbf{y}_e$ normal to the equivalent plane must be zero.

$$\mathbf{x_o} \cdot \mathbf{y_e} = \cos \lambda_s \cos \phi_n \sin \eta_s \cos \eta_e - \sin \lambda_s \cos \eta_s \cos \eta_e + \cos \lambda_s \sin \phi_n \sin \eta_e = 0 \tag{10}$$

From Eqs. (7) and (10), shear flow angle is given by (Merchant, 1944)

$$\tan \eta_s = \frac{\tan \lambda_s \cos(\phi_n - \gamma_n) - \tan \eta_c \sin \phi_n}{\cos \gamma_n} \tag{11}$$

Substituting Eqs. (7) and (11) into Eqs. (8) and (9), the components can be simplified to

$$\mathbf{x_o} = (\cos\phi_n \cos\lambda_s \cos\eta_s + \sin\lambda_s \sin\eta_s)\mathbf{x_e} - (\cos\lambda_s \sin\phi_n / \cos\eta_e)\mathbf{z_e} \quad (12)$$

$$\mathbf{z_c} = (\sin(\phi_n - \gamma_n)\cos\eta_c \cos\eta_s - \sin\eta_c \sin\eta_s)\mathbf{x_e} + (\cos(\phi_n - \gamma_n)\cos\eta_c / \cos\eta_e)\mathbf{z_e} \quad (13)$$

A one-dimensional approach is used to take account of the steady state flow condition. In the case, all the quantities of the cutting process in the primary shear zone are only dependent on the coordinate z_e. Therefore, the components of material velocity in the primary shear zone are defined by

$$\mathbf{v} = v_{x_e}(z_e)\mathbf{x_e} + v_{z_e}(z_e)\mathbf{z_e} \quad (14)$$

The tangential velocity components with the boundary conditions are given below

$$\begin{cases} \mathbf{v}|_{z_e=0} = \mathbf{V} = -V\mathbf{x_o} = V(-(\cos\phi_n \cos\lambda_s \cos\eta_s + \sin\lambda_s \sin\eta_s)\mathbf{x_e} \\ \qquad\qquad + (\cos\lambda_s \sin\phi_n / \cos\eta_e)\mathbf{z_e}) \\ \mathbf{v}|_{z_e=h} = \mathbf{V_c} = V_c\mathbf{z_c} = V_c((\sin(\phi_n - \gamma_n)\cos\eta_c \cos\eta_s - \sin\eta_c \sin\eta_s)\mathbf{x_e} \\ \qquad\qquad + (\cos(\phi_n - \gamma_n)\cos\eta_c / \cos\eta_e)\mathbf{z_e}) \end{cases} \quad (15)$$

where V_c is chip velocity, h is thickness of the primary shear zone.The velocity field must satisfy the assumption of plastic incompressibility (Johnson and Mellor, 1983). Consequently, it obeys the following equation.

$$\frac{\partial v_{x_e}}{\partial x_e} + \frac{\partial v_{z_e}}{\partial z_e} = 0 \quad (16)$$

Since the velocity field is expressed as function of z_e, the normal velocity component is constant.

$$\frac{\partial v_{z_e}}{\partial z_e} = 0 \Rightarrow v_{z_e} = const = v_{z_e}|_{z_e=0} = v_{z_e}|_{z_e=h} = V_n = \frac{V\cos\lambda_s \sin\phi_n}{\cos\eta_e} \quad (17)$$

According to the continuity condition of Eq. (17), the chip velocity is obtained (Usui et al., 1978).

$$V_c = V\frac{\cos\lambda_s \sin\phi_n}{\cos\eta_c \cos(\phi_n - \gamma_n)} \quad (18)$$

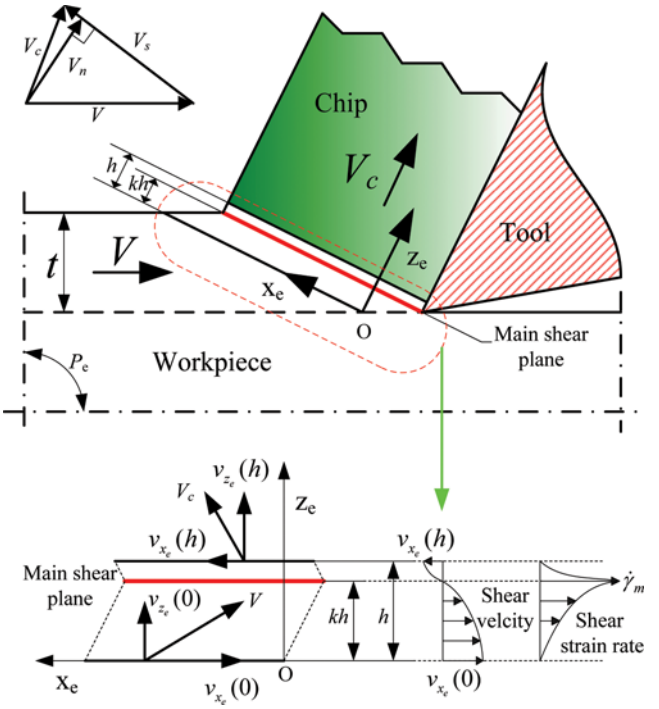

FIGURE 4 Unequal division shear zone model. (Figure available in color online.)

The shear velocity of chip is

$$\mathbf{V_s} = \mathbf{v}|_{z_e=h} - \mathbf{v}|_{z_e=0} = \mathbf{V_c} - \mathbf{V} = (v_{x_e}(h) - v_{x_e}(0))\mathbf{x_e}$$
$$= \frac{V \cos\lambda_s \cos\gamma_n}{\cos\eta_s \cos(\phi_n - \gamma_n)}\mathbf{x_e} \tag{19}$$

The velocities of cutting (V), chip (V_c), shear (V_s) create a velocity triangle in equivalent plane P_e as shown in Figure 4.

GOVERNING EQUATIONS OF THE PRIMARY SHEAR ZONE

The governing equations of workpiece material flow through the primary shear zone are analyzed under the following assumptions:

- Viscoplastic workpiece material: the workpiece material is supposed to be homogeneous and isotropic, and governed by Johnson-Cook constitutive equation.
- Continual chip formation process: the chip formation is supposed to occur mainly by shearing in the primary shear zone.

- Steady state flow: it is assumed that all the variables in the primary shear zone are independent on the time.
- One-dimensional condition: these physical quantities defining the cutting process are expressed as functions of one coordinate z_e. This coordinate is perpendicular to the primary shear band.
- Sharp cutting edge: as the undeformed chip thickness is high enough, the edge effects on cutting forces can be neglected.
- Constant thickness of the primary shear zone: the primary shear zone is modeled as a shear band of constant thickness.

Material Model

Johnson-Cook (JC) constitutive equation is often used as flow stress model of work material in modeling machining operations due to its accuracy and simplicity. This material model is given as

$$\tau = \frac{1}{\sqrt{3}}\left[A + B\left(\frac{\gamma}{\sqrt{3}}\right)^{n}\right]\left[1 + C\ln\left(\frac{\dot{\gamma}}{\dot{\gamma}_0}\right)\right]\left[1 - \left(\frac{T - T_r}{T_m - T_r}\right)^{m}\right] \tag{20}$$

where γ is the shear plastic strain, $\dot{\gamma}$ is the shear stain rate, $\dot{\gamma}_0$ is reference plastic strain rate, T is instantaneous temperature of the workpiece material, T_r and T_m are room temperature and melting temperature respectively, A, B, C, n, m are the material constants.

Governing Equations of Strain, Strain Rate, and Shear Velocity

In the equivalent plane $P_e(\mathbf{x_e}, \mathbf{z_e})$, the compatibility condition (Johnson and Mellor, 1983) relates the shear strain rate to velocity field.

$$\dot{\gamma} = \dot{\gamma}_{z_e x_e} = \frac{dv_{x_e}}{dz_e} + \frac{dv_{z_e}}{dx_e} = \frac{dv_{x_e}}{dz_e} \tag{21}$$

Note that the shear strain rate is also the material derivative of the shear strain (Johnson and Mellor, 1983). For the steady-state flow condition of a continuous chip, the strain variation is independent of the time. So, the partial time derivative of strain vanishes, thus

$$\dot{\gamma} = \frac{d\gamma}{dt} = \frac{\partial\gamma}{\partial t} + \frac{\partial\gamma}{\partial z_e}\frac{\partial z_e}{\partial t} = \frac{\partial\gamma}{\partial t} + V_n\frac{\partial\gamma}{\partial z_e} = V_n\frac{d\gamma}{dz_e} = \frac{V\cos\lambda_s\sin\phi_n}{\cos\eta_e}\frac{d\gamma}{dz_e} \tag{22}$$

The commonly used model for the primary zone is parallel-sided shear zone model proposed by Oxley (1989). In Oxley's model, the main shear plane is assumed to be equidistant from the entry boundary and the exit boundary. Astakhov et al. (2001) thought the shear zone can be divided

into two unequal regions by using the microstructure experiment of a single chip fragment. Tounsi et al. (2002) identified the material constants of JC constitutive equation using the unequal division shear zone model. In this paper, the orthogonal cutting theory based on unequal division shear zone model (Li et al., 2011) is extended to oblique cutting, as shown in Figure 4.

In the tests performed by Oxley (1989), the strain rate increased with increase in cutting speed and had a maximum value occurred in the middle of the primary shear zone. The strain rate at entry boundary between the shear zone and workpiece and the exit boundary between the shear zone and chip is zero approximately. So, a piecewise power law distribution assumption of the shear strain rate is proposed (see Figure 4), it is expressed as

$$\dot{\gamma} = \begin{cases} \frac{\dot{\gamma}_m}{(kh)^q} z_e^q & z_e \in [0, kh] \\ \frac{\dot{\gamma}_m}{(1-k)^q h^q} (h - z_e)^q & z_e \in [kh, h] \end{cases} \tag{23}$$

where $\dot{\gamma}_m$ is the maximum strain rate. k is unequal division ratio. q is a parameter characterizing the non-uniform distribution of the tangential velocity in the deformation zone.

Equations (21) and (22) can be combined and integrated with respect to z_e with the boundary conditions that the shear strain is zero at the entry boundary of primary shear zone ($\gamma|_{z_e=0} = 0$). The relationship between the velocity and strain is obtained.

$$v_{x_e} = (V \cos\lambda_s \sin\phi_n / \cos\eta_e)\gamma - V(\cos\lambda_s \cos\phi_n \cos\eta_s + \sin\lambda_s \sin\eta_s) \tag{24}$$

Equations (22) and (23) are combined and integrated with respect to z_e, the shear strain distribution is then given as

$$\gamma = \begin{cases} \frac{\dot{\gamma}_m \cos\eta_e}{(q+1)V\cos\lambda_s \sin\phi_n (kh)^q} z_e^{q+1} & z_e \in [0, kh] \\ -\frac{\dot{\gamma}_m \cos\eta_e}{(q+1)V\cos\lambda_s \sin\phi_n (1-k)^q h^q} (h - z_e)^{q+1} + \frac{\cos\gamma_n \cos\eta_e}{\cos(\phi_n - \gamma_n)\cos\eta_s \sin\phi_n} & z_e \in [kh, h] \end{cases} \tag{25}$$

Substituting Eq. (25) into (24) gives

$$v_{x_e} = \begin{cases} \frac{\dot{\gamma}_m}{(q+1)(kh)^q} z_e^{q+1} - V(\cos\lambda_s \cos\phi_n \cos\eta_s + \sin\lambda_s \sin\eta_s) & z_e \in [0, kh] \\ -\dfrac{\dot{\gamma}_m}{(q+1)(1-k)^q h^q} (h - z_e)^{q+1} & \\ \quad + \dfrac{V\cos\lambda_s \sin\phi_n}{\cos(\phi_n - \gamma_n)} (\sin(\phi_n - \gamma_n)\cos\eta_s - \tan\eta_c \sin\eta_s) & z_e \in [kh, h] \end{cases} \tag{26}$$

Comparing the tangential component of the cutting velocity at the entry boundary with the tangential component of chip velocity at the exit boundary, we notice a change of its sign (see Figure 4). The main shear plane is assumed to be the plane where the tangential velocity is equal to zero.

$$v_{x_e}|_{z_e=kh} = 0 \tag{27}$$

The solutions of Eq. (27) are expressed as

$$k = \frac{\cos(\phi_n - \gamma_n)\cos\eta_s(\cos\phi_n\cos\eta_s + \tan\lambda_s\sin\eta_s)}{\cos\gamma_n} \tag{28}$$

$$\dot{\gamma}_m = \frac{(q+1)V\cos\lambda_s\cos\gamma_n}{h\cos\eta_s\cos(\phi_n - \gamma_n)} \tag{29}$$

Substituting Eqs. (28) and (29) into (23), (25) and (26) finally gives the shear strain rate, shear strain, and shear velocity distribution in the primary zone.

Governing Equations of Temperature

In cutting process, the boundary of the primary shear zone can be considered adiabatic, the thermal conductivity is then negligible (Komanduri and Hou, 2000). Assuming that a fraction μ (Taylor-Quinney coefficient) of the plastic work is converted into heat, since the temperature depends only on the coordinate z_e under the steady flow condition, consequently, the heat transfer equation becomes

$$\frac{dT}{dz_e} = \frac{\cos\eta_e}{\rho c V\sin\phi_n\cos\lambda_s}\mu\tau\dot{\gamma} \tag{30}$$

where ρ, c, and μ represent material density, heat capacity, and Taylor-Quinney coefficient, respectively. T is instantaneous temperature of the chip.

The thermal boundary condition have to be specified: the chip temperature at the entry boundary is equal to the initial workpiece temperature or room temperature.

$$T|_{z_e=0} = T_w \tag{31}$$

The material behavior and thermomechanical evolution in the primary shear zone are governed by the Eqs. (20), (23), (25) and (30). Due to γ and $\dot{\gamma}$ are functions of z_e, τ is a function of z_e and T, which is known from

Eq. (20). So Eq. (30) is a first-order ordinary differential equation for the unknowns T and z_e. The equation can be easily solved by numerical integration method, and then the temperature distribution is obtained. Substituting the results into Eq. (20), the shear stress distribution across the primary shear zone and the shear stress τ_s on the main shear plane can also be calculated.

CUTTING FORCE CALCULATION OF OBLIQUE CUTTING

For oblique cutting, F_c (cutting force), F_d (back force), and F_f (feed force) are, respectively, the components of the resultant cutting force $\mathbf{F}$ in the direction of unit vectors $\mathbf{x_o}$, $\mathbf{y_o}$, and $\mathbf{z_o}$, as shown in Figure 2. The resultant force $\mathbf{F}$ is expressed as in ($\mathbf{x_o}$, $\mathbf{y_o}$, $\mathbf{z_o}$) system

$$\mathbf{F} = -F_c\mathbf{x_o} - F_d\mathbf{y_o} + F_f\mathbf{z_o} \tag{32}$$

F_s and F_{ns} represent shear force and normal force on the main shear plane respectively. Stabler (1951) made an assumption that the shear force is collinear with the shear velocity, which is considered as one of maximum shear stress criteria. Therefore, $\mathbf{F}$ can be rewritten in ($\mathbf{x_s}$, $\mathbf{y_s}$, $\mathbf{z_s}$) system

$$\begin{aligned}\mathbf{F} &= -F_s\mathbf{x_s} + F_{ns}\mathbf{z_s} = -F_s\cos\eta_s\mathbf{x} + F_s\sin\eta_s\mathbf{y} + F_{ns}\mathbf{z}\\ &= -(F_s(\cos\eta_s\cos\phi_n\cos\lambda_s + \sin\eta_s\sin\lambda_s) + F_{ns}\sin\phi_n\cos\lambda_s)\mathbf{x_o}\\ &\quad - (F_s(\cos\eta_s\cos\phi_n\sin\lambda_s - \sin\eta_s\cos\lambda_s) + F_{ns}\sin\phi_n\sin\lambda_s)\mathbf{y_o}\\ &\quad - (F_s\cos\eta_s\sin\phi_n - F_{ns}\cos\phi_n)\mathbf{z_o}\end{aligned} \tag{33}$$

F_{nc} and F_{fc}, respectively, denoted the normal force and friction force at the tool-chip interface, the mean friction coefficient is defined by

$$f = \tan\beta = \frac{F_{fc}}{F_{nc}} \tag{34}$$

where f is mean friction coefficient, β is mean friction angle.

From experimental observations, Armarego and Brown (1969) assumed that the friction force acting on the tool rake face is collinear with the chip velocity. The resultant force $\mathbf{F}'$ of the tool-chip interface face corresponds to

$$\begin{aligned}\mathbf{F}' &= F_{nc}\mathbf{x_c} - F_{fc}\mathbf{z_c} = F_{nc}\mathbf{x_c} - F_{nc}\tan\beta\mathbf{z_c}\\ &= F_{nc}(\cos(\phi_n - \gamma_n) - \tan\beta\sin(\phi_n - \gamma_n)\cos\eta_c)\mathbf{x} - F_{nc}\tan\beta\sin\eta_c\mathbf{y}\\ &\quad - F_{nc}(\sin(\phi_n - \gamma_n) + \tan\beta\cos(\phi_n - \gamma_n)\cos\eta_c)\mathbf{z}\end{aligned} \tag{35}$$

In the steady cutting process, the equilibrium of the forces applied to the chip reduces to

$$\mathbf{F} + \mathbf{F}' = 0 \tag{36}$$

The following expressions were deduced by Moufki et al. (2000) by substituting Eqs. (33) and (35) into Eq. (36).

$$\tan \eta_s = \frac{\tan \beta \sin \eta_c}{\cos(\phi_n - \gamma_n) - \tan \beta \sin(\phi_n - \gamma_n) \cos \eta_c} \tag{37}$$

$$F_{nc} = \frac{\cos \eta_s}{\cos(\phi_n - \gamma_n) - \tan \beta \sin(\phi_n - \gamma_n) \cos \eta_c} F_s \tag{38}$$

$$F_{ns} = (\sin(\phi_n - \gamma_n) + \tan \beta \cos \eta_c \cos(\phi_n - \gamma_n)) F_{nc} \tag{39}$$

On the basis of equality between Eqs. (11) and (37), Moufki et al. (2000) led to an implicit equation from which the chip flow angle η_c was calculated.

$$\begin{aligned} &\tan \eta_c \sin \phi_n \cos(\phi_n - \gamma_n) - \sin \eta_c \tan \beta \sin \phi_n \sin(\phi_n - \gamma_n) \\ &\quad - \tan \lambda_s \cos^2(\phi_n - \gamma_n) + \cos \eta_c \tan \lambda_s \tan \beta \sin(\phi_n - \gamma_n) \cos(\phi_n - \gamma_n) \\ &\quad + \sin \eta_c \tan \beta \cos \gamma_n = 0 \end{aligned} \tag{40}$$

Assuming the shear stress distribution on the main shear plane is considered as uniform, the shear force F_s is proportional to the shear stress τ_s (Usui et al., 1978). Then

$$F_s = \frac{\tau_s}{\cos \lambda_s \sin \phi_n} tb \tag{41}$$

The cutting force components (F_c, F_d, F_f) are given as by combining Eqs. (32) and (33).

$$\begin{pmatrix} F_c \\ F_d \\ F_f \end{pmatrix} = \begin{pmatrix} \cos \eta_s \cos \phi_n \cos \lambda_s + \sin \eta_s \sin \lambda_s & \sin \phi_n \cos \lambda_s \\ \cos \eta_s \cos \phi_n \sin \lambda_s - \sin \eta_s \cos \lambda_s & \sin \phi_n \sin \lambda_s \\ -\cos \eta_s \sin \phi_n & \cos \phi_n \end{pmatrix} \begin{pmatrix} F_s \\ F_{ns} \end{pmatrix} \tag{42}$$

The normal shear angle ϕ_n can be calculated using Merchant's formula.

$$\phi_n = \frac{\pi}{4} - \frac{\beta}{2} + \frac{\gamma_n}{2} \tag{43}$$

As suggested by Schulz (1996), the mean friction coefficient may be a power function of the chip velocity.

$$f = f_0 V_c^p \tag{44}$$

where f_0 is constant, f is mean friction coefficient, $p < 0$.

CUTTING FORCE MODEL FOR END MILLING

Cutter Geometrical Model

From previous works (Altintas, 2000a), the global geometry of the end milling cutter is described in Figure 5. The milling parameters are defined in a local coordinate system (**x, y, z**). The cutting edges lie on the tool envelope surface which consists of a cylindrical surface with a radius r. Each cutting edge is considered as a helix with a constant helix angle λ_s. The local cutting edge geometry and the three differential cutting forces at the cutting points (i.e., P in Figure 5) along the cutting edge are identified by axial elevation z and peripheral rotation angle θ.

For the local point P, at the sth discrete point (height z) on the cutting edge referenced j, is located by its angular position ϕ_{js} measured from the y-axis and defined by:

$$\phi_{js} = \theta - \Delta\phi + (j-1)\phi_P = \theta - \frac{z}{r}\tan\lambda_s + (j-1)\frac{2\pi}{N} \tag{45}$$

where N is the number of cutting edges and θ is the tool rotation angle measured positively from the y-axis around the z-axis. ϕ_p is pitch angle between the phase of first cutting edge and next one, it is determined by the number of flutes. Because the end milling has a helix angle flute, the helix angle may cause a three-dimensional cutting effect that can be considered small differential oblique cutting process. Then, there is some phase difference between the cutting edge on the upper and the one on the lower. The phase difference may cause a phase lag angle about $\Delta\phi$. Lag angle $\Delta\phi$ between upper and lower edges has a relationship with the axis depth z, cutter radius r, and cutting edge helix angle λ_s.

As shown in Figure 6, the instantaneous undeformed chip thickness can be written as the following.

$$t = f_t \sin(\phi_{js})\Gamma_{js} = (f_{\mathrm{m}}/n_r N)\sin(\phi_{js})\Gamma_{js} \tag{46}$$

where f_t is the feed per tooth, and it is determined from $f_m/(n_r N)$. n_r represents spindle speed, f_m is the feed per minute.

All the locations of discrete points on the cutting edges are calculated in terms of Eq. (45). Finding the cutter-workpiece engagement domain is

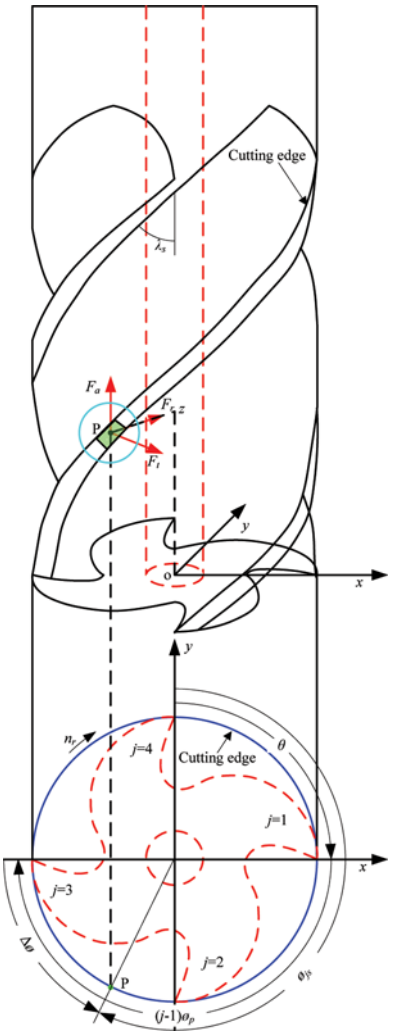

FIGURE 5 Geometric model of end milling cutter. (Figure available in color online.)

very critical, it affects the cutting force calculations directly. Because the discrete cutting edge points of the cutter are engaged with the workpiece at any instant of machining time, it contributes a portion of cutting forces. Therefore, engagement recognition factor is defined by

$$\Gamma_{js} = \begin{cases} 1 & \phi_{st} \le \phi_{js} \le \phi_{ex} \left(\begin{array}{l} \text{if the } s\text{th discrete point on the} \\ j\text{th cutting edge is in engagement with workpiece} \end{array} \right) \\ 0 & \phi_{js} < \phi_{st} \text{ or } \phi_{js} > \phi_{ex} (\text{otherwise}) \end{cases} \tag{47}$$

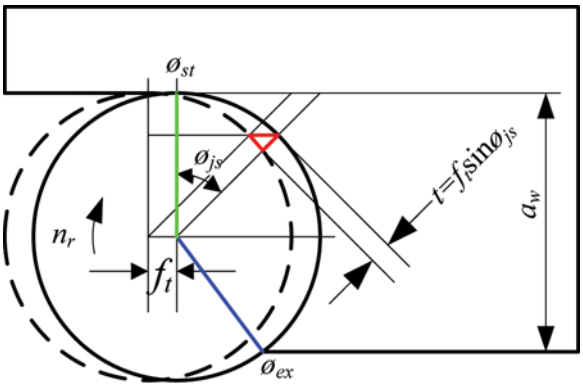

FIGURE 6 Instantaneous undeformed chip thickness. (Figure available in color online.)

Cutting Force Model

The tool edge is decomposed into a series of small differential oblique cutting elements. For a differential cutting edge at the *s*th discrete point on the *j*th cutting edge, which is in engagement domain, the oblique cutting method proposed by us is used to predict the differential cutting forces. The differential shear cutting force (dF_s) on the main shear plane can be written as follows based on the oblique cutting model from Eq. (41)

$$dF_s = \frac{\tau_s t}{\cos\lambda_s \sin\phi_n} db \tag{48}$$

where db represents differential cutting width along the longitudinal cutter axis at the *k*th discrete point on the *j*th cutting edge, and it is determined from d$b = a_w/K \cdot a_w$ and K are cutting width and total number of discrete points on a cutting edge.

The differential normal cutting force (dF_{ns}) perpendicular to the main shear plane is deduced from relations (38) and (39) by the force equilibrium on the chip

$$dF_{ns} = \frac{\cos\eta_s(\tan(\phi_n - \gamma_n) + \tan\beta\cos\eta_c)}{(1 - \tan\beta\cos\eta_c\tan(\phi_n - \gamma_n))} dF_s \tag{49}$$

The shear and normal cutting forces (dF_s, dF_{ns}) of differential oblique cutting edge at the *s*th discrete point on the *j*th cutting edge can be transformed into tangential, radial and axial differential cutting forces respectively (dF_r, dF_t, dF_a). At these differential elements having depth db may also

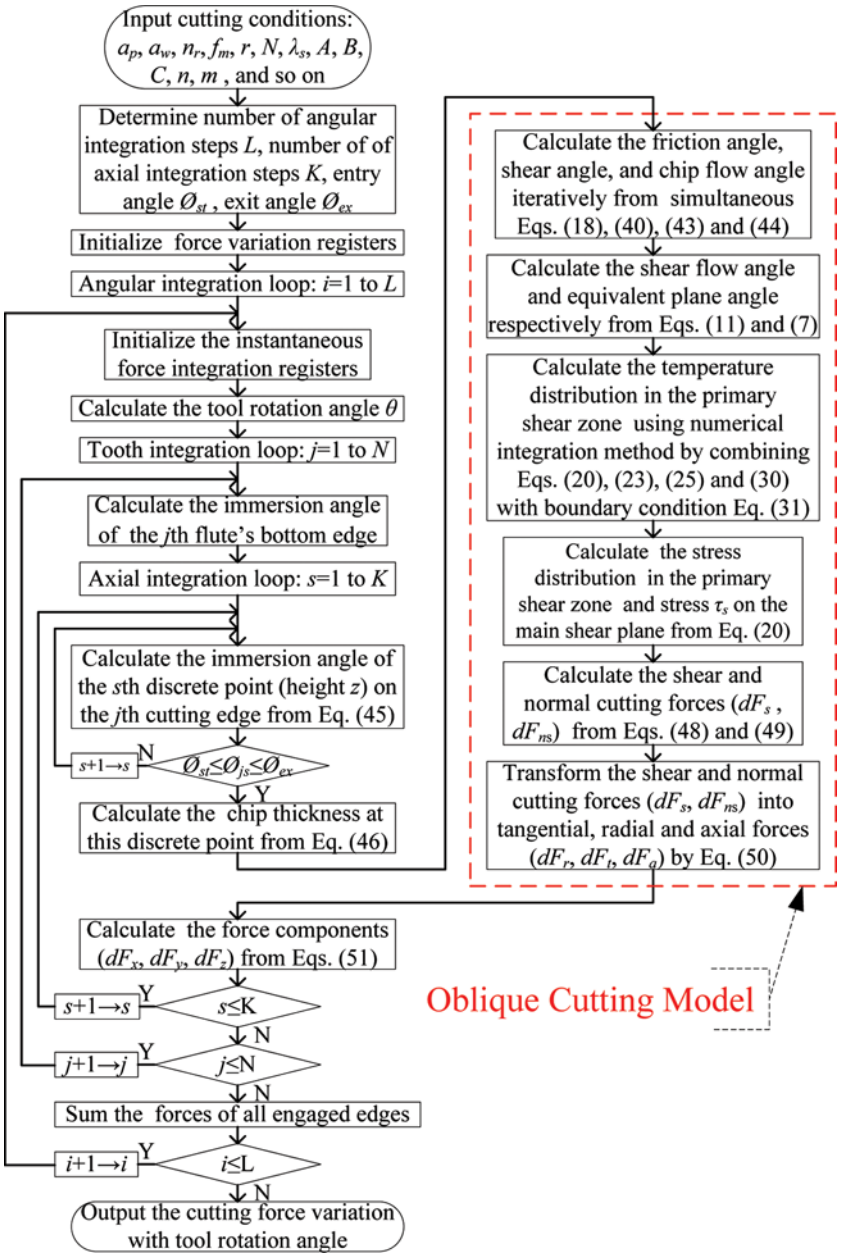

FIGURE 7 Flow chart for the oblique cutting theory applied to end milling. (Figure available in color online.)

be rewritten in the following equations by Eq. (42).

$$\begin{pmatrix} dF_t \\ dF_r \\ dF_a \end{pmatrix} = \begin{pmatrix} \cos\eta_s \cos\phi_n \cos\lambda_s + \sin\eta_s \sin\lambda_s & \sin\phi_n \cos\lambda_s \\ \cos\eta_s \cos\phi_n \sin\lambda_s - \sin\eta_s \cos\lambda_s & \sin\phi_n \sin\lambda_s \\ -\cos\eta_s \sin\phi_n & \cos\phi_n \end{pmatrix} \begin{pmatrix} dF_s \\ dF_{ns} \end{pmatrix} \quad (50)$$

The cutting forces in **x, y** and **z** direction at the small differential elements may also be transformed as the following

$$\begin{pmatrix} dF_x \\ dF_y \\ dF_z \end{pmatrix} = \begin{pmatrix} -\cos\phi_{js} & \sin\phi_{js} & 0 \\ \sin\phi_{js} & -\cos\phi_{js} & 0 \\ 0 & 0 & 1 \end{pmatrix} \begin{pmatrix} dF_t \\ dF_r \\ dF_a \end{pmatrix} \quad (51)$$

By integrating Eq. (51) respectively, the total cutting force in each direction can be obtained. The algorithm for predicting the cutting forces in end milling is outlined in Figure 7.

$$\begin{pmatrix} F_x \\ F_y \\ F_z \end{pmatrix} = \sum_{j=1}^{N} \sum_{s=1}^{K} \begin{pmatrix} dF_x \\ dF_y \\ dF_z \end{pmatrix} \Bigg|_{j,s} \quad (52)$$

RESULTS AND DISCUSSION

Oblique Cutting Validation of 42CrMo4

The effectiveness of the proposed method is verified by the experimental data of oblique cutting test published by Moufki et al. (2004) for 42CrMo4. Material constants and thermo-physical properties of workpiece are given by

$A = 612\,\text{MPa}$, $B = 426\,\text{MPa}$, $C = 0.008$, $n = 0.15$, $m = 1.46$, $\dot{\gamma}_0 = 0.001\,1/\text{s}$, $T_m = 1800\,\text{K}$, $T_r = 300\,\text{K}$, $\rho = 7800\,\text{kg/m}^3$, $\lambda = 54\,\text{W/(m K)}$, $c = 500\,\text{J/(kg K)}$

The flow stress data is identified by Moufki et al. (2004) through quasi-static and high strain rate compression tests.

Because it is difficult to measure the thickness of the shear zone accurately under the different conditions of machining, so a typical value of $h = 0.025\,\text{mm}$ (Show, 1984) was taken in the present calculation. The same methodology is also was taken used by Moufki et al. (2004). Fiction coefficient in metal cutting is usually larger that measured in conventional sliding friction tests. It is well-known that the friction coefficient decreases with the cutting speeds over a narrow range. The simple empirical relation (44)

gives interesting information on a non-constant friction coefficient at the tool-chip interface. f_0 is reference friction coefficient measured at a cutting speed. p shows that the decreasing effect of cutting speed on the friction. It was found that $f_0 = 0.704$ and $p = -0.248$ from the literature (Dudzinski and Molinari, 1996). Because the cutting speed is not enough high, q is set to 3 (Li et al., 2011).

Table 1 lists the detail of predicted cutting force, feed force and back force with the experimental data of Moufki et al. (2004) for 42CrMo4.

Figure 8 shows the comparison of forces predicted by proposed model for 42CrMo4 steel with experimentally measured forces of Moufki et al. (2004). Although there is some difference between the predictions and experiments, the trend in force is in good agreement. The main causes of the severe discrepancy between the theoretical and experimental results are accounted for

- *Effects of tool edge radius*. The predicted forces are calculated assuming that the tool edge is perfectly sharp. Whereas practically all cutting tools have some finite edge radius, the cutting edge contributes some amount of ploughing force.
- *Friction effects*. The mean friction coefficient depends on the chip velocity, temperature and normal stress on the tool-chip interface. Nevertheless, the empirical relation (44) only takes account of the chip velocity. In fact, cutting process generates more heat when increasing cutting thickness, the temperature of the tool-chip interface rises, the mean friction coefficient is reduced.
- *Effects of shear angle*. In the shear angle theories, many equations were proposed, but it is still unclear which equation is the most suitable. That explains the small discrepancy observed here.
- *Effects of shear zone thickness*. Because it is difficult to measure the thickness of the shear zone under different conditions of machining accurately, this paper used a typical value, $h = 0.025$ mm. In fact, the shear zone thickness becomes wider with the increase of cutting thickness.
- *Effects of material constants*. Johnson-Cook flow stress data of 42CrMo4 steel was identified through quasi-static and high strain rate compression tests (Moufki et al., 2004) where the range of strain, strain rate and temperature appear to be limited.

As depicted in Figure 9, the cutting forces are influenced by cutting parameters as well as tool geometry. The influence of these parameters on the force components are analysed as follows.

- *Cutting thickness, t*. Taking no account of the influence of cutting thickness on the friction, the increase of cutting forces is proportionate to

TABLE 1 Results of Predictions and Experiments (Moufki et al., 2004) of Oblique Cutting for 42CrMo4 ($\gamma_n = 0°$, $b = 3$ mm)

Test number	Inclination Angle λ_s (°)	Cutting Velocity V (m/min)	Cutting Thickness t (mm)	Measured Cutting Force F_c (N)	Predicted Cutting Force F_c (N)	Measured Feed Force F_f (N)	Predicted Feed Force F_f (N)	Measured Back Force F_d (N)	Predicted Back Force F_d (N)
1	5	60	0.10	920	849	714	703	33	48
2	5	60	0.15	1202	1294	821	1099	48	69
3	5	120	0.10	930	784	639	563	28	41
4	5	120	0.15	1160	1158	715	811	40	64
5	5	240	0.10	800	706	530	415	22	39
6	5	240	0.15	1004	1047	590	601	34	61
7	5	480	0.10	758	647	503	311	17	37
8	5	480	0.15	970	962	590	454	32	58
9	10	60	0.10	882	828	686	652	86	104
10	10	60	0.15	1115	1292	715	1091	90	140
11	10	120	0.10	789	787	572	566	65	82
12	10	120	0.15	1037	1162	698	815	80	128
13	10	240	0.10	756	709	555	417	48	78
14	10	240	0.15	1000	1050	622	604	56	121
15	10	480	0.10	706	649	490	313	38	75
16	10	480	0.15	900	964	507	456	50	117

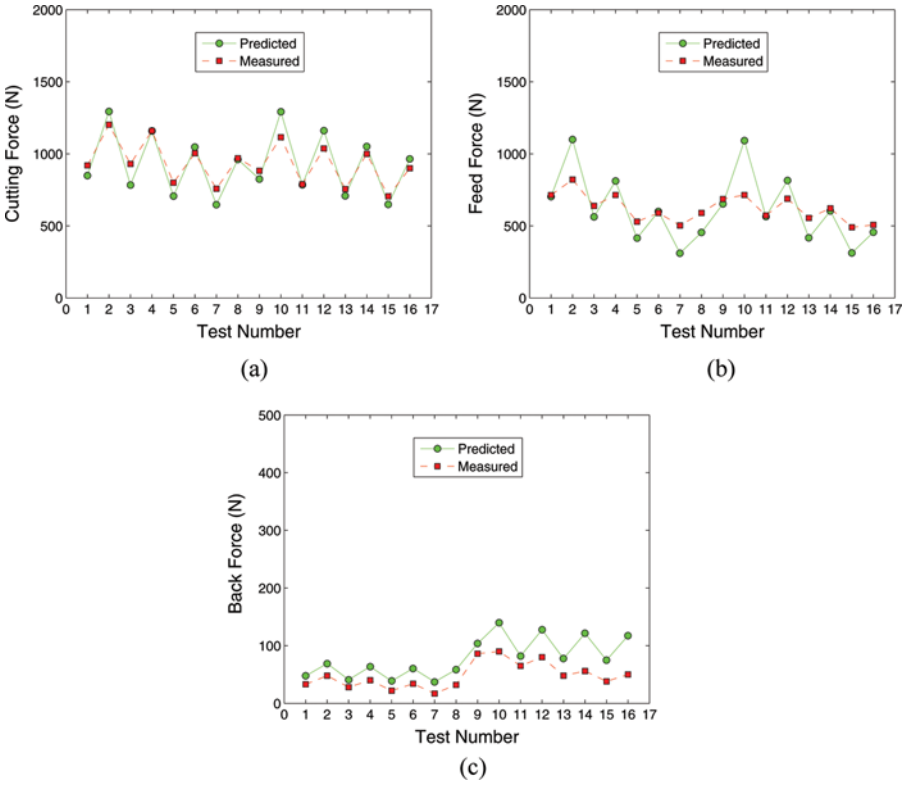

FIGURE 8 Comparison of predicted cutting force (a), feed force (b), and black force (c) with the experimental data of Moufki et al. (2004) 42CrMo4. (Figure available in color online.)

that of cutting chip thickness, as shown in Figure 9(a). But as a matter of fact, the increase of cutting thickness generates more heat, which again leads to the decrease of cutting forces with the reduced friction coefficient.

- *Cutting speed, V.* In the range of medium speed, the cutting forces decrease while the cutting speed increase, as Figure 9(b) shows.
- *Edge inclination angle,* λ_s. From Figure 9(c), we note that cutting force and feed force is independent of edge inclination angle, however, back force increasing with the increase in the edge inclination angle. Such tendency is in agreement with the results of Lin et al. (1982).

In the cutting process, the workpiece material becomes the chip mainly by shearing within the primary deformation zone, the evolution of workpiece material is very complex under the extremely intense conditions of high strain, strain rate and temperature. The simulation results in Figure 10(b) indicated that the temperature increases with the increase of the shear strain (see Figure 10(a)), which is attributed to plastic

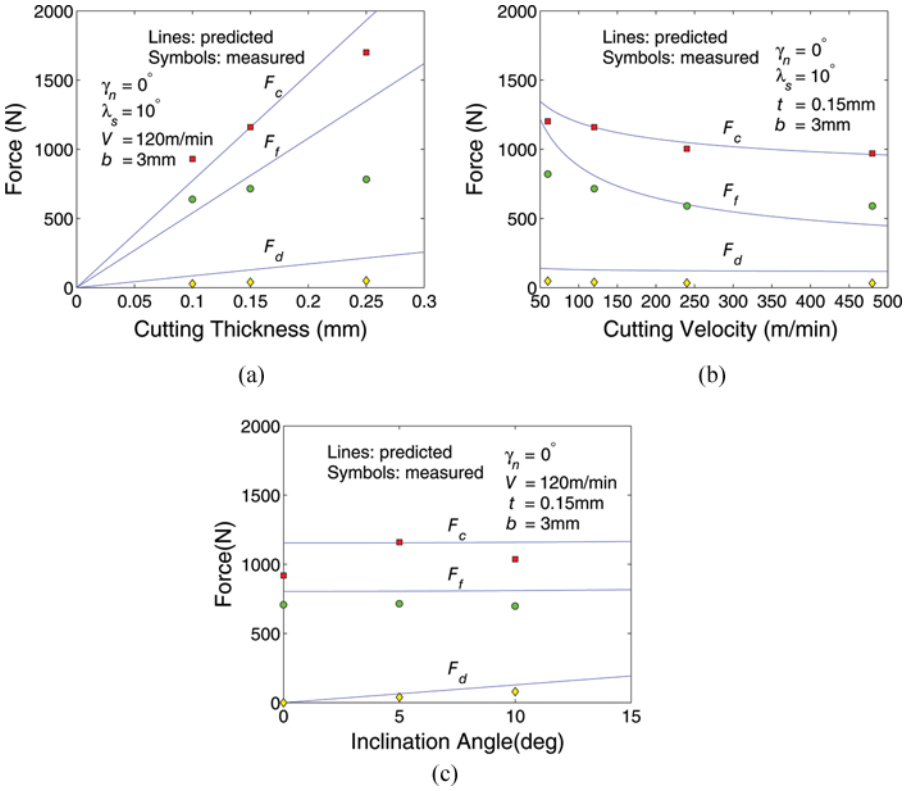

FIGURE 9 Comparison between predicted and measured force for 42CrMo4 (Moufki et al., 2004) versus cutting thickness (a), cutting velocity (b), and edge inclination angle (c). (Figure available in color online.)

deformation work generating more heat. The chip temperature rises by about 200°K through the shear zone, which is in good agreement with Komanduri's results (2000). Shear stress in Figure 10(c) shows a trend of first increase and then decrease with the chip strain and temperature increasing, which is up to a maximum value on the main shear plane. One possible reason is that the rise of temperature has more influence of thermal softening than work hardening of strain increase on the workpiece material.

End Milling Application of AISI 1045

The application of the proposed oblique cutting model to end milling is explored. The experimental setup is presents in Figure 11. Twenty-six cutting tests under various cutting conditions were performed on Mikron UCP 800 vertical milling machine. A set of representative milling tests were listed in Table 2. The workpiece material is a block of AISI 1045 steel of which

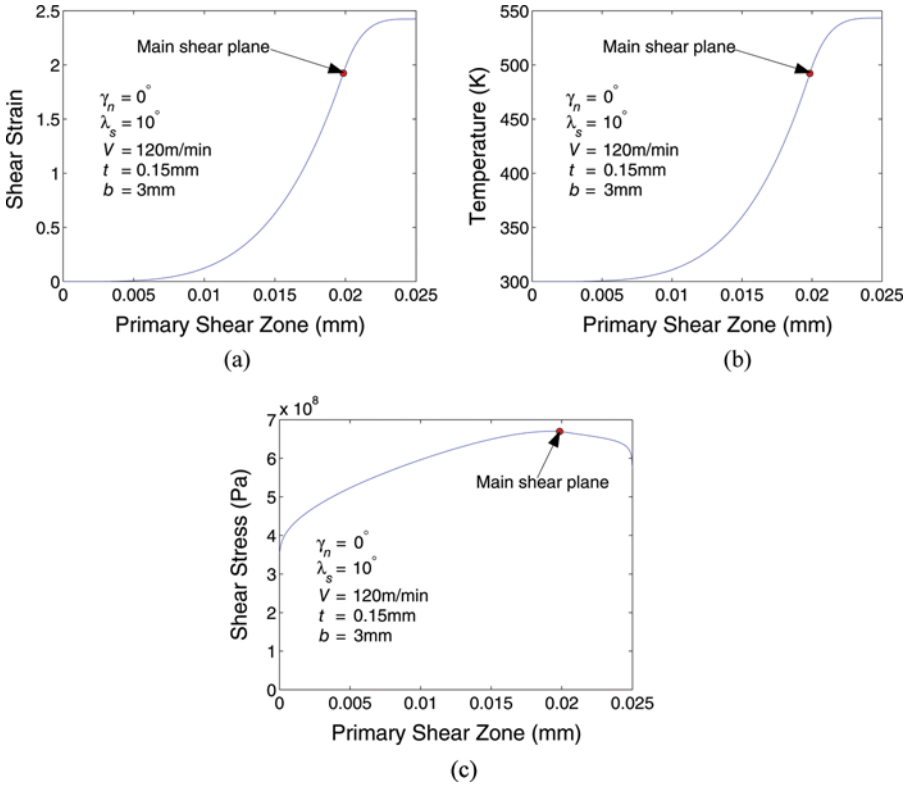

FIGURE 10 Predicted results of the shear strain (a), temperature (b), and shear stress (c) distribution in the primary shear zone. (Figure available in color online.)

Johnson-Cook flow stress data was (Adibi-Sedeh, 2003): $A = 553\,\text{MPa}$, $B = 600\,\text{MPa}$, $C = 0.0134$, $n = 0.234$, $m = 1$, $\dot{\gamma}_0 = 0.00\,1/\text{s}$ (unit of shear strain rate $[\text{s}-1]$), $T_m = 1733\,\text{K}$, $T_r = 300\,\text{K}$. Thermophysical properties of workpiece material are given by $\rho = 7800\,\text{kg/m}^3$, $\lambda = 47\,\text{W/(m K)}$, $c = 423\,\text{J/(kg K)}$. Other simulated parameters is considered as same as those of

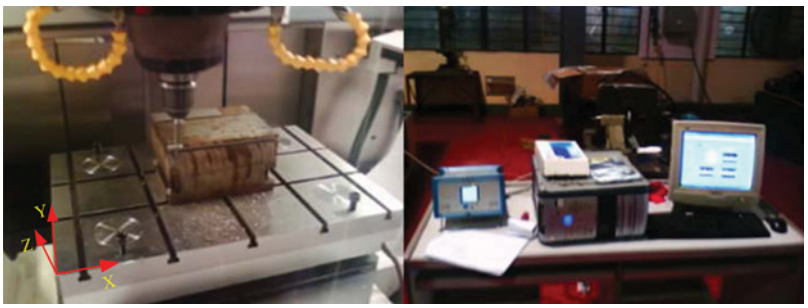

FIGURE 11 Experimental configuration of end milling. (Figure available in color online.)

TABLE 2 Cutting Parameters for End Milling Tests and Simulations

	Test Number			
Cutting Parameters	1	2	3	4
Cutting depth a_p/mm	5	5	5	5
Cutting width a_w/mm	2	4	4	4
Spindle speed n_r/(r/min)	600	600	600	1200
Feed rate f_t/(mm/z)	0.02	0.02	0.04	0.02

42CrMo4 for the calculus carried out for analyzing the consistency of the model. A three-fluted HSS end mill with a nominal diameter of 16 mm, a nominal helix angle of 30° and a radial normal rake angle of 15° was used in the experiments. The cutter was traveled along a linear toolpath. All cutting experiments were up milling. The tests were conducted without cutting fluid and the cutting forces were measured with a six-component Kistler table dynamometer (Kistler 9523B).

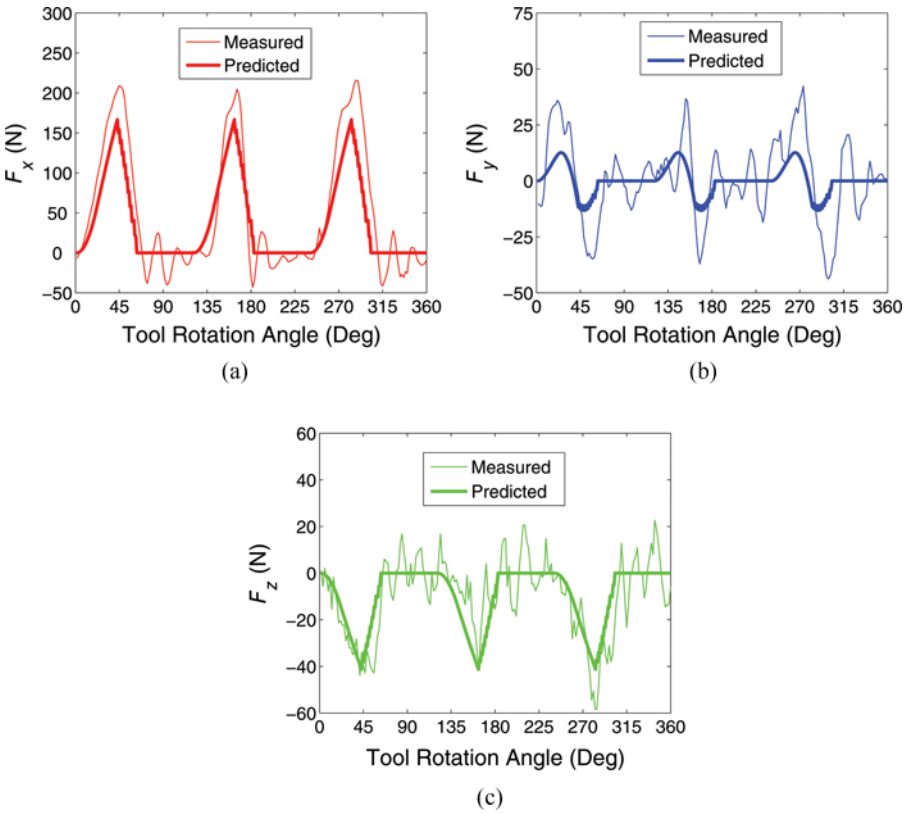

FIGURE 12 Comparison of measured and predicted cutting force for test 1. (Figure available in color online.)

The program of cutting force simulations for end milling was all executed with Matlab7.0 on a computer. The flow chart of the program may be shown in Figure 7. In the simulations, the cutter was discretized into 10 disks (calculation increments on z as $db = 0.5$ mm), the force calculations were performed every 1 degrees of cutter rotation (calculation increments on θ as $d\theta = 1°$).

The measured and predicted cutting forces with the proposed model for the investigated cutting conditions are shown in Figures 12–15. In general, a good agreement is observed between the measurements and corresponding simulations. There is a small amount of amplitude discrepancy between the predictions and the experiments. Since the model developed here considers the cutting tool as rigid, this discrepancy might be due to cutting tool deflections. Cutting deflection may contribute to the variations in the instantaneous chip thickness (Smith and Tlusty, 1991).

In addition, there is another factor which is difficult to avoid: the tool run-out. In milling, this geometrical default is mainly due to the offset

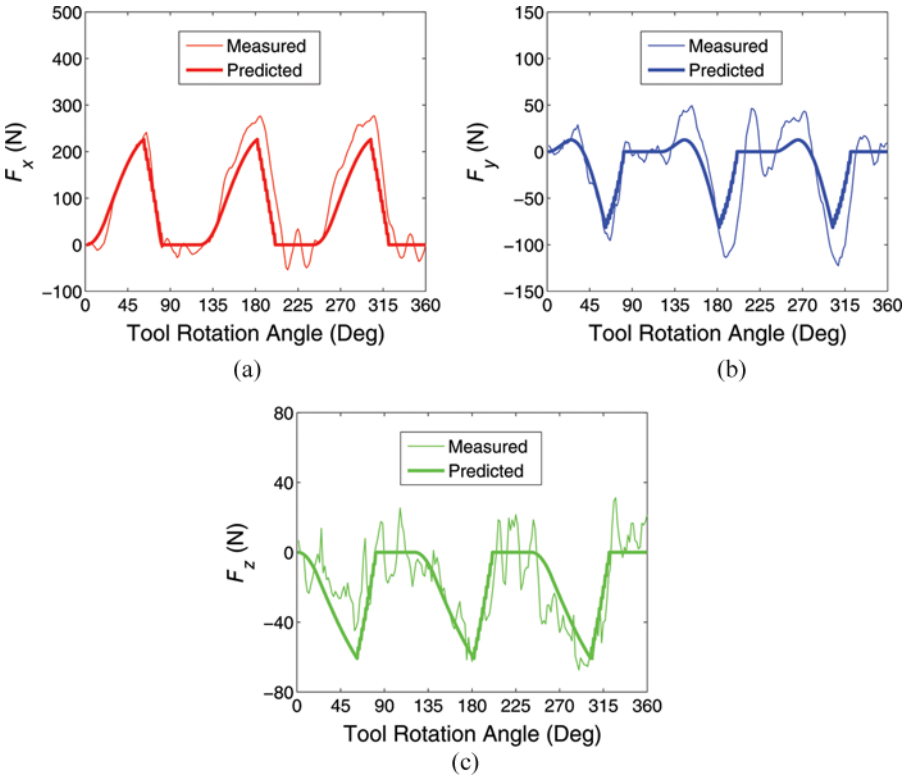

FIGURE 13 Comparison of measured and predicted cutting force for test 2. (Figure available in color online.)

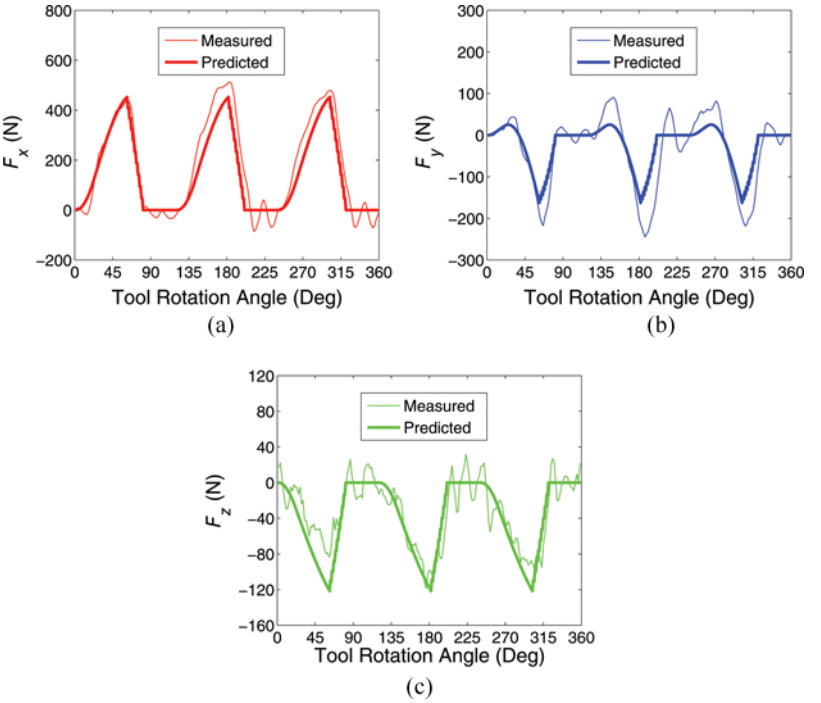

FIGURE 14 Comparison of measured and predicted cutting force for test 3. (Figure available in color online.)

between the position of the tool rotation axis and the spindle rotation axis (Fontaine et al., 2006). The consequence is a tool rotation around the spindle axis with an eccentricity. This eccentricity modifies the tool engagement and the local cutting conditions (cutting velocity and angles). Then, the run-out has a direct effect on the cutting forces level and variation. Its effect is particularly significant when the undeformed chip thickness t reaches small values, as shown in Figure 12.

Influence of cutting conditions on cutting force: (1) Feed per teeth f_t. It can be noted that the feed rate variation affects directly the cutting forces, indeed these values depend proportionally on the undeformed chip thickness t. Figures 13 and 14 show the three force components maximum values double closely as the feed per teeth increases from 0.02 mm/z to 0.04 mm/z. In milling parameters, f_t has the greatest effect on cutting force. (2) Cutting width a_w. a_w influences the cutting force by changing the immersion angles of start and exit. In the experiment, the immersion angle of entry was constantly set to zero. Figures 12 and 14 show the cutting forces for the various immersion angles of exit. When cutting width increases from 2 mm to 4 mm, the immersion angles of exit change from 41° to 60°. So cutting forces increase with the cutter-worpiece engagement

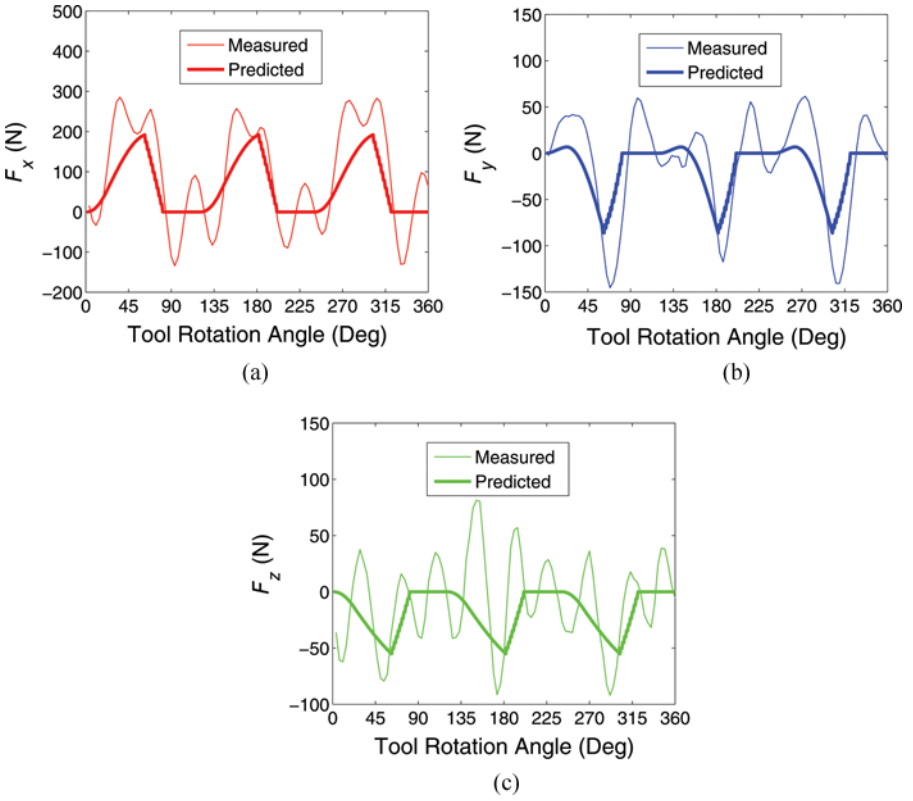

FIGURE 15 Comparison of measured and predicted cutting force for test 4. (Figure available in color online.)

domain expansion. However, the increase of cutting width is disproportionate to that of cutting forces.

Cutting width has a relatively large effect on the force components F_y (normal to feed direction), as shown in Figures 12(b) and 13(b). (3) spindle speed n_r. Comparing the predicted force components in Figures 13 and 15, the global level of cutting forces decreases theoretically with increasing values of spindle speed, which is accounted for by Equation (44). This is because of the synchronous increase in the cutting speed and spindle speed, consequently friction coefficient decreases, the temperature at tool-chip interface rises, flow stress reduce to respond to thermal softening effect. But actual observations show no obvious changes in the measured force amplitude (see Figures 13 and 15). In fact, the cutting forces level is greatly influenced by tool vibration and run-out especially when the spindle speed goes up. Some observations in Figures 13 and 15 confirmed an evident difference in measured cutting forces between the two spindle speeds.

CONCLUSIONS

In this article, an analytical method based on unequal division shear zone model is proposed to study the machining predictive theory in oblique cutting. The proposed model modifies previous idea of equal division shear zone. To establish governing equation of chip flow through the primary shear zone, a piecewise power law distribution assumption of shear strain rate is introduced. While computing the flow stress, the strain, strain rate, and temperature effects are taken into consideration. Oblique cutting test data for 42CrMo4 steel from available literature is used to verify the present work.

End milling is here modelled by using the proposed analytical approach of oblique cutting. The helical flutes are divided into small differential oblique cutting edge. Milling force is obtained by summing oblique cutting forces. The detailed algorithm of the proposed model application to practical end milling is described. A set of tests for AISI 1045 steel under different cutting conditions was introduced and used to validate the proposed model. The predicted results give a good approximation for the forces and the main experimental tendencies. The proposed model allows us to analyze the effects of different cutting conditions as feed rate or cutting width on cutting force level. This model is useful to simulate the cutting process in order to enhance machining quality.

The proposed model requires only workpiece material properties and cutting conditions without additional experimental data of orthogonal cutting. It can easily be extended to other workpiece material and machining operations such as turning and drilling.

ACKNOWLEDGMENTS

This work is supported by the National Basic Research (973) Program of China (Grant No. 2009CB724306).

NOMENCLATURE

V	cutting velocity
t	cutting thickness
b	cutting width
γ_n	normal rake angle
λ_s	inclination angle
ϕ_n	normal shear angle
η_e	equivalent plane angle
η_c	chip flow angle

η_s	shear flow angle
$\mathbf{v}$	flow velocity of material in the primary shear zone
v_{x_e}, v_{z_e}	components of material velocity in the x_e and z_e directions
V_c	chip velocity
V_n	normal velocity
V_s	shear velocity
τ	shear stress
τ_s	flow stress in the main shear plane
γ	shear strain
$\dot{\gamma}$	shear strain rate
$\dot{\gamma}_m$	maximum strain rate in the main shear plane
$\dot{\gamma}_0$	reference plastic strain rate
T	instantaneous temperature of the chip
T_r	room temperature
T_w	initial workpiece temperature
T_m	melting temperature
μ	taylor-Quinney coefficient,
β	mean friction angle at the tool-chip interface
f	mean friction coefficient
0, p	constants of friction coefficient
A, B, C, n, m	material constants
ρ	material density
λ	meat conductivity coefficient
c	meat capacity
q	parameter of strain rate distribution
k	unequal division ratio of primary shear zone
h	thickness of the primary shear zone
$\mathbf{F}$, $\mathbf{F}'$	resultant forces applied to chip by workpiece and tool, respectively
F_s, F_{ns}	shear and normal force in the main shear plane
F_{fc}, F_{nc}	friction and normal force at the tool-chip interface
F_c, F_d, F_f	components of resultant force $\mathbf{F}$ in the $\mathbf{x_o}$, $\mathbf{y_o}$, and $\mathbf{z_o}$ direction
F_x, F_y, F_z	components of resultant cutting force for end milling
ϕ_{js}	instantaneous immersion angle
ϕ_{st}	cutter entry angle
ϕ_{ex}	cutter exit angle
θ	cutter rotation angle
ϕ_P	pitch angle between the phase of first cutting edge and next one
$\Delta\phi$	lag angle
i, j, s	serial numbers of rotation angle, cutting edge, and discrete point of milling cutter
f_m	feed per minute
f_t	feed per tooth
n_r	spindle speed
a_w	cutting width for end milling

a_p	cutting depth for end milling
r	radius of milling cutter
N	number of cutting edges
Γ_{js}	engagement recognition factor

REFERENCES

Adibi-Sedeh, A.H.; Madhavan, V.; Bahr, B. (2003) Extension of Oxley's analysis of machining to use different material models. *Journal of Manufacturing Science and Engineering*, 125: 656–666.

Altintas, Y. (2000a) *Manufacturing Automation*, Cambridge University Press, Cambridge, UK.

Altintas, Y. (2000b) Modeling approaches and software for predicting the performance of milling operations at MAL-UBC. *Machining Science and Technology*, 4: 445–478.

Armarego, E.J.A.; Brown, R.H. (1969) *The Machining of Metals*, Prentice-Hall, Englewood Cliffs, NJ.

Armarego, E.J.A.; Whitfield, R.C. (1985) Computer based modeling of popular machining operations for force and power predictions. *Annals of the CIRP*, 34: 65–69.

Astakhov, V.P.; Osman, M.O.M.; Hayajneh, M.T. (2001) Re-evaluation of the basic mechanics of orthogonal metal cutting: Velocity diagram, virtual work equation, and upper bound theorem. *International Journal of Machine Tools and Manufacturing*, 41: 393–418.

Budak, E.; Altintas, Y.; Armarego, E.J.A. (1996) Prediction of milling force coefficients from orthogonal cutting data. *Journal of Manufacturing Science and Engineering*, 118: 216–224.

Budak, E.; Ozlu, E. (2008) Development of a thermomechanical cutting process model for machining process simulations. *CIRP-Manufacturing Technology*, 57(1): 97–100.

Dudzinski, D.; Molinari, A. (1997) A modelling of cutting for viscoplastic materials. *International Journal of Mechanical Sciences*, 39(4): 369–389.

Fontaine, M.; Devillez, A.; Moufki, A.; Dudzinski, D. (2006) Predictive force model for ball-end milling and experimental validation with a wavelike form machining tests. *International Journal of Machine Tools & Manufacture*, 46: 367–380.

Johnson, W.; Mellor, P.B. (1983) *Engineering Plasticity*, John Wiley & Sons, New York.

Komanduri, R.; Hou, Z.B. (2000) Thermal modeling of the metal cutting process, Part I: Temperature rise distribution due to shear plane heat source. *International Journal of Mechanical Sciences*, 42: 1715–1752.

Lazoglu, I. (2003) Sculpture surface machining: a generalized model of ball-end milling force system. *International Journal of Machine Tools & Manufacture*, 43: 453–562.

Li, B.L.; Wang, X.L.; Hu, Y.J. (2011) Analytical prediction of cutting forces in orthogonal cutting using unequal division shear-zone model. *International Journal of Advanced Manufacturing Technology*, 54: 431–443.

Lin, G.C.I.; Mathew, P.; Oxley, P.L.B. (1982) Predicting cutting forces for oblique machining conditions. *Proceedings of the Institution of Mechanical Engineers*, 196: 141–148.

Lin, Z.C.; Lin, Y.Y. (1999) A study of an oblique cutting model. *Journal of Materials Processing Technology*, 86: 119–130.

Llanos, I.; Villar, J.A.; Urresti, I.; Arrazola, P.J. (2009) Finite element modeling of oblique machining using an arbitrary Lagrangian-Eulerlan formulation. *Machining Science and Technology*, 13: 385–406.

Merchant, M.E. (1944) Basic mechanics of the metal cutting process. *Journal of Applied Mechanics*, (11)A: 168–175.

Morcos, W.A. (1980) A slip line field solution of the free continuous cutting problem in conditions of light friction at chip-tool interface. *Journal of Engineering for Industry*, 102: 310–314.

Moufki, A.; Devillez, A.; Dudzinski, D.; Molinari, A. (2004) Thermomechanical modelling of oblique cutting and experimental validation. *International Journal of Machine Tools and Manufacturing*, 44: 971–989.

Moufki, A.; Dudzinski, D.; Molinari, A.; Rausch, M. (2000) Thermomechanical modelling of oblique cutting forces and chip flow prediction. *International Journal of Mechanical Sciences*, 42: 1205–1232.

Oxley, P.L.B. (1989) *Mechanics of Machining*, Ellis Horwood, Chichester, UK.

Rao, B.; Shin, Y.C. (2002) Analysis of three-dimensional machining using an extended oblique machining theory. *Machining Science and Technology*, 6: 187–213.

Sabberwal, A.J.P. (1960) Chip section and cutting force during the end milling operation. *Annals of the CIRP*, 10(3): 197–203.

Schultz, H. (1996) *High-Speed Machining*, Munich, Carl Hanser.

Shamoto, E.; Altintas, Y. (1999) Prediction of shear angle in cutting with maximum shear stress and minimum energy principles. *Journal of Manufacturing Science and Technology*, 121: 399–407.

Shaw, M.C. (1984) *Metal Cutting Principles*, Oxford University Press, Oxford, UK.

Shaw, M.C.; Cook, N.H.; Smith, P.A. (1952) The mechanics of three-dimensional cutting operations. *Transactions of the ASME*, 74: 1055–1064.

Smith, S.; Tlusty, J. (1991) An overview of modeling and simulation of the milling process. *Journal of Engineering for Industry*, 113: 16–175.

Stabler, G.V. (1951) Fundamental geometry of cutting tools. *Proceedings of the Institution of Mechanical Engineers*, 165: 14–21.

Stephenson, D.A.; Wu, S.M. (1988) Computer models for the mechanics of three-dimensional cutting processes, Part I: Theory and numerical method. *Journal of Engineering for Industry*, 110: 32–37.

Tounsi, N.; Vincenti, J.; Otho, A.; Elbestawi, M.A. (2002) From the basic of orthogonal metal cutting toward the identification of the constitutive equation. *International Journal of Machine Tools and Manufacturing*, 42(2): 1373–1383.

Usui, E.; Hirota, A.; Masuko, M. (1978) Analytical predictions of three dimensional cutting process. Part 1: basic cutting model and energy approach. *Journal of Engineering for Industry*, 100: 222–228.

Yang, M.Y.; Park, H.D. (1991) The prediction of cutting forces in ball-end milling. *International Journal of Machine Tools & Manufacture*, 31: 45–54.

Yun, W.S; Cho D.W. (2001) Accurate 3-D cutting force prediction using cutting condition independent coefficients in end milling. *International Journal of Machine Tools & Manufacture*, 41: 463–478.